THE ISOCAM DARK CURRENT CALIBRATION REPORT

A. Biviano[1,2], M. Sauvage[3], P. Gallais[3], P. Roman[1]
B. Altieri[1], O. Boulade[3], S. Guest[1], L. Metcalfe[1], K. Okumura[1], S. Ott[1],

1: CAM IDT, ESA Satellite Tracking Station, PO Box 50727, E-28080 Madrid, Spain
2: Osservatorio Astronomico di Trieste, via G.B. Tiepolo 11, I-34131 Trieste, Italy
3: CEA, DSM/DAPNIA/SAp, CE-Saclay, F-91191, Gif-sur-Yvette Cedex, France

Version 1.2 – May 18^{th}, 1998

Abstract

We describe the calibration, measurements and data reduction, of the dark current of the ISO-CAM LW and SW detectors. We point-out the existence of two significant drifts of the LW dark-current, one throughout the ISO mission, on a timescale of days, another within each single revolution, on a timescale of hours. We also show the existence of a dependence of the dark current on the temperature of the CAM detector.

By characterizing all these effects through polynomial fittings, we build a model for the LW calibration dark, that depends on the epoch of observation (parametrized with the revolution number and the time elapsed in that given revolution since the activation) and on the temperature of the CAM detector. The model parameters are tuned for each of CAM-LW pixel.

We show that the modelling is very effective in taking into account the dark-current variations and allows a much cleaner dark subtraction than using a brute average of several calibration dark images.

The residuals of the LW model-dark subtraction are, on average, similar to the pre-launch expectation. This is also the case for the SW detector, in which case, though, only a simple average of several dark-current observations has been used to produce the calibration dark.

1 Introduction

In this document we describe the calibration of the dark current in the ISO-CAM LW and SW detectors.

The SW dark current is dominated by tunnel effects, while the LW dark current is due to thermal charge generation in the photoconductors and charge leakage generated during the commutation of the reset transistor (see "The ISOCAM Observer's Manual"). The LW dark frame shows a line pattern with a clear separation between odd and even lines (see an example of a dark frame taken at T_{int} =2 s in Fig. 1).

During the ISO mission it was shown that the LW dark-current is drifting both on a timescale of hours within a given revolution, and on a timescale of days throughout the

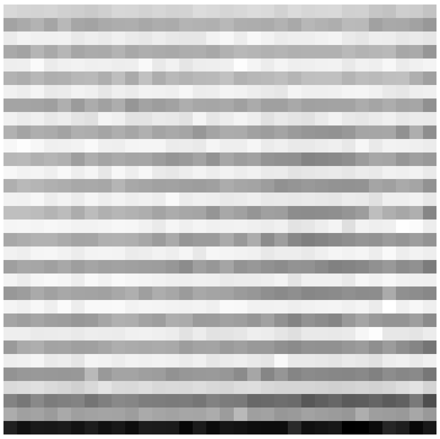

Figure 1: An example of the LW dark frame, measured at T_{int} =2 s. Note the very evident line pattern.

mission. Hereafter we will refer to these drifts as the *short-term* and *long-term* trends of the dark current.

The dark currents have been calibrated with four different kinds of observations:

- Darks measured during calibration-dedicated revolutions, i.e. those that are specifically dedicated to calibration observations (typically, one per week); we call these measurements the *calibration darks.*
- Darks measured during the handover period, i.e. when the satellite tracking switches from one of the two antennae (VILSPA or Goldstone) to the other (this time typically lasts 15–30 min every revolution); we call these measurements the *handover darks.*
- Darks measured during the deactivation period (lasting typically 1 hour every revolution) i.e. when ISO enters the Earth radiation belts and scientific observations are no longer possible because of the high rate of glitch impacts, just before all instruments have to be switched off; we call these measurements the *deactivation darks.*
- Darks measured in the CAM parallel mode of observation, i.e. taking advantage of the part of telemetry (1/12) that is reserved to CAM when other ISO instruments are observing in prime mode; we call these measurements the *parallel-mode darks.*

The four types of dark measurements have different goals. The *calibration darks* are long measurements done throughout the mission to constrain the pattern of the dark frame, i.e. the dark current variation from one pixel to another. The *calibration darks* are measured at regularly spaced time intervals, typically one measure at all T_{int} every month. These time intervals are not so dense as to allow a very clean characterization of the long-term drifts of the dark currents. On the other hand, specific repeated observations of the dark current throughout the same revolution allow to constrain the short-term drift (as we will see, see § 5).

A proper characterization of the long-term drifts is provided by the *handover darks*, which are shorter (and therefore noisier) measurements done at every revolution, throughout the whole ISO mission, and more or less at the same time after the activation of the instrument. Unfortunately, the limited time available during the handover sequence imposed severe constraints on the measurements, and it was decided to monitor only two T_{int} (2 and 5 s) LW darks during handover. Only recently, i.e. starting from revolution 764 (december 1997), the handover sequence of dark measurements has been changed in order to monitor also the 0.28 and 10 s LW darks, as it was understood that the long-term drift was important, and it was necessary to check that the drift was the same (or at least similar) at different T_{int} (see § 3).

Since revolution 764, the even days are dedicated to the measurements of darks at T_{int} =0.28 and 10 s, and the odd days to the darks at T_{int} =2 and 10 s. The dark at T_{int} =20 s is not covered, for obvious reasons of time limitation (notice that CAM observations at T_{int} =20 s are strongly affected from glitches, so that this T_{int} is very seldom used by observers).

The *deactivation darks* include LW dark measurements at T_{int} =2 and 5 s and SW dark measurements at T_{int} =6 s. One could think that the *deactivation darks* provide a monitoring of the long-term trend of the dark currents. Unfortunately, these *deactivation darks* are strongly affected by the so-called *space weather,* i.e. particles in the Earth environment (for further details, see Gallais 1998). This is quite unfortunate, because it has the consequence that we must rely on *calibration darks* for constraining the SW dark long-term behaviour, as no SW dark measurement is done during handover (because of the limited time available), but *calibration darks* are not measured in every revolution.

Most of the measurements of *parallel-mode darks* were done in the last seven months of the ISO mission. Based on the repeated measurements of *calibration darks* in a single revolution, the short-term drift of the LW dark current was discovered. As a consequence, a denser time monitoring of the LW dark current was required. In order to have more measurements, and to avoid using too much calibration time, it was decided to have dark measurements with CAM in the parallel mode. Even with the reduced telemetry rate available, these measurements have since proven to be extremely useful to constrain the dark drifts within single revolutions. These measurements have been done at all LW T_{int} , with the exception of T_{int} =0.28 s, unfeasible because of a software limitation in the total number of frames that can be accumulated on-board. However, several *calibration darks* have been measured at this particular T_{int} to fill this gap.

2 Dark data-reduction

The data-reduction of dark measurements consists in deglitching, and averaging (or taking the median) of the stabilized frames.

2.1 Deglitching

Deglitching is always a very complicated operation for CAM observations. Several deglitching methods are used for the dark measurements[1], but typically the most used are *TCOR, TEMP,* and *MM,* all methods implemented in the *CAM Interactive Analysis* software package (Ott et al. 1996, Delaney 1997, Claret 1998).

The *TEMP* method of deglitching has been used in the early times of the ISO mission for the data-reduction of *calibration darks*, while the *MM* method has been used in the most recent times. The two methods provide essentially identical results. More specifically, we can quantify the difference as follows. After deglitching the same set of dark frames with the two methods, we subtracted one of the resulting dark image from the other; the residuals of this subtraction quantify the importance of using two different methods of deglitching. The average residual difference (over all pixels) is less than 0.005 ADUs[2], with an RMS of 0.04 ADUs and the maximum difference is 0.16 ADU.

On the other hand, the *TCOR* method has been used for the deglitching of *handover darks* (Gallais 1998), and it does give slightly different results from the previous two methods. The final dark images as obtained from the same data-set but with either the *TCOR*

[1] The reason why different methods of data-reductions have been adopted for different dark measurements is historical and we will not discuss it here.

[2] Dark measurements are sometimes done with a gain factor ×1, and sometimes with a gain factor ×2. Here and in the rest of this document, all units are scaled by the gain factor *even if not explicitely indicated* – i.e. both "ADU" and "ADU/G" mean Analog-to-Digital Units scaled by the gain factor.

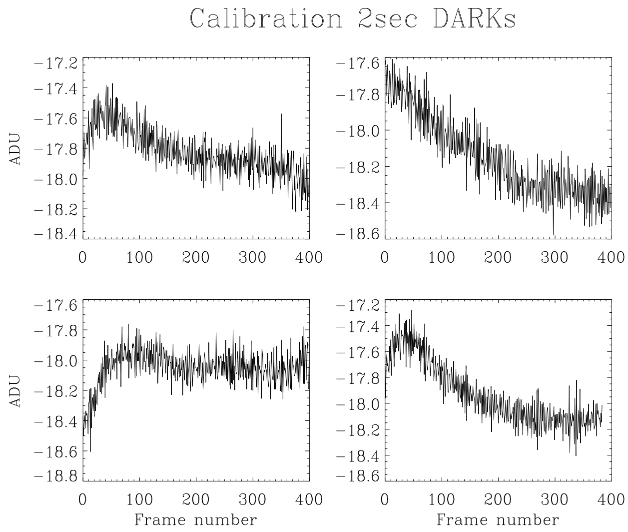

Figure 2: The mean current vs. frame number in four *calibration darks* measurements at T_{int} =2 s. Note the slow stabilization drifts.

deglitching method, or the *MM* one, differ by, on average, 0.07 ADU, with an RMS of 0.12 and a peak difference of 0.34 ADUs. These differences arise from the lower deglitching efficiency of the *TCOR* method (see also Claret 1998). Since faint glitches are not detected by the *TCOR* method, yet they are detected by the *TEMP* or the *MM* ones, and glitches always contribute a spurious positive signal, the resulting dark level after deglitching is always sistematically higher when the *TCOR* method is used.

Luckily, the *handover darks* are only used for establishing a linear trend over long timescales (see § 3) and the good statistics (*handover darks* are measured every day) compensates for the additional noise induced by an imperfect deglitching. The overall positive offset of the mean level of *handover darks* is not a problem, as it can be corrected using the *calibration darks* and/or the *parallel-mode darks* (see § 5).

2.2 Stabilization

As the CAM detector has a slow response to flux variations, it takes some time for a CAM pixel to level off to the dark level from a pre-existing condition of illumination. Often, even in very long dark measurements, stabilization is not achieved. As an example of different beahviours, we show in Fig. 2 the mean dark level vs. the frame number in four *calibration darks* measurements at T_{int} =2 s. After an initial increase, due to the change of integration time from a previous dark measurement, the dark level slowly decreases to its stabilized value. It is clear that only the last frames can be used to form the final image.

As an additional example, we show in Fig. 3 the handover dark measurements at 2 and 5 s T_{int} , i.e. the mean current level measured in the LW CAM detector vs. the frame number. In the T_{int} =2 s dark measurement, one can see the initial decrease due to the fact that CAM was open before the dark measurement; in the T_{int} =5 s dark measurement, one can see the current change due to the change in T_{int} , followed by another long period of stabilization to the level of the dark current at T_{int} =5 s.

Finally, we give in Fig. 4 four examples of *parallel-mode darks*. As above, we plot the mean current level vs. the frame number to show the stabilization trend. Generally, the fact

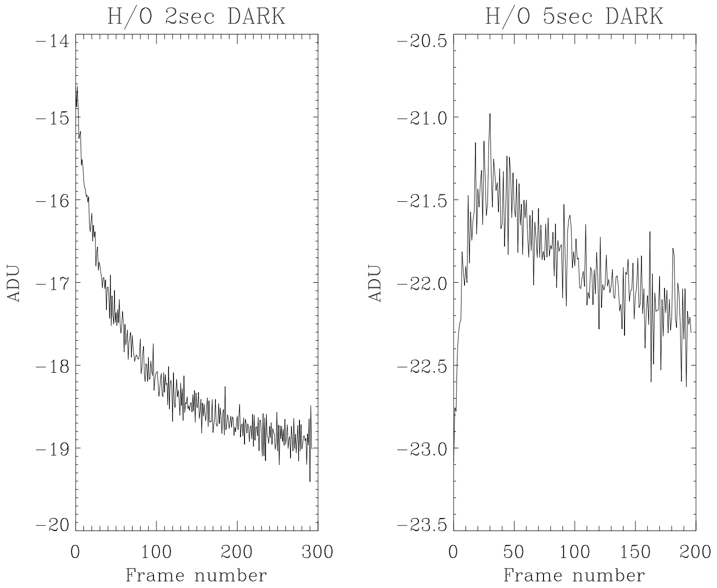

Figure 3: The mean current vs. frame number in two *handover darks* measurements at T_{int} =2 and 5 s. Note the slow stabilization drifts.

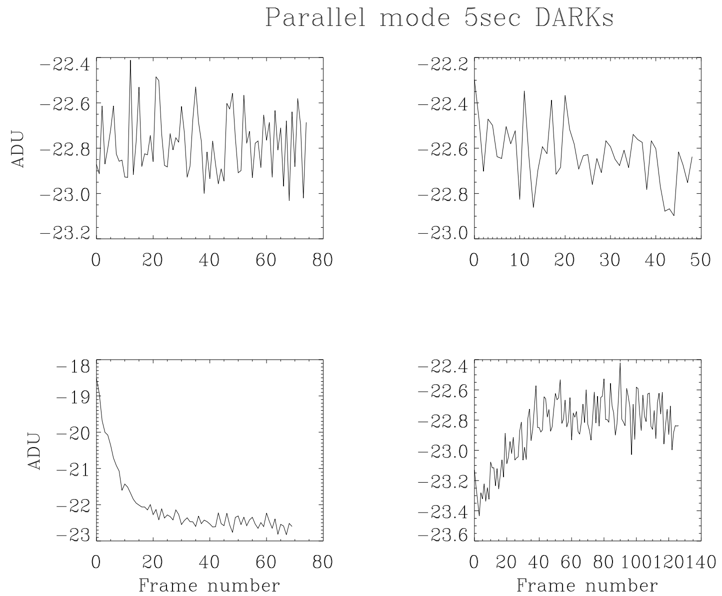

Figure 4: The mean current vs. frame number in four *parallel-mode darks* measurements at T_{int} =5 s. Note the slow stabilization drifts.

that the CAM detector is kept in the same dark configuration during the whole revolution (except for the handover interval) means that stabilization should not be a problem here. However, after handover there is a stabilization drift (this is shown in the lower-left panel of Fig. 4), and additional drifts (of much lower importance, though) arise because of the change in the CAM detector temperature, which is affected by the operations of other ISO instruments (see § 4).

The criteria for choosing the stabilized frames may be slightly different for the three kinds of measurements. In particular, the choice of the stabilized frames of the *calibration darks* cannot be blind, as these measurements are not always done in the same conditions of previous illumination of the CAM detector (e.g., the dark measurement can happen after the observation of a calibrating star, or after a parallel mode configuration); depending on what was the previous CAM target, the stabilization trend can be quite different. On the other hand, *parallel-mode darks* are always very close to stabilization, so that, after excluding the frames measured just after the handover, all frames can be used to build the dark image, by taking their median. Finally, since the measurements of *handover darks* are always done in the same way, the data-reduction procedure is automatic, and only the last 10 frames are averaged to give the final dark image (see Gallais 1998). This choice can produce a different mean dark current level for *handover darks* as compared to *calibration darks* and *parallel-mode darks*. However, this offset can be (and is) corrected (see § 5).

3 Long-term drift

The *handover darks* provide an excellent constraint on the long-term drift of the LW dark current. The mean value of the T_{int} =2 and 5 s *handover darks* are shown in Fig. 5 and Fig. 6, respectively, from revolution 150 to 829 (the handover dark measurements started to be done routinely in revolution 150). There is a clear decreasing trend of the dark current, approximately linear with the revolution number. However, the trend is not the same over the whole array, as can be seen in the figures, where the mean values of the odd and even line pixels are shown separately. A proper characterization of this trend must therefore take into account individual pixels.

For each pixel, we made a linear fit of the dark current drift with revolution. The histograms of the individual pixel long-term drifts are shown in Fig. 7 and Fig. 8. It can be seen that the drift is (on average) more negative for even-line pixels than for odd-line pixels, for both T_{int} , and ranges from ~ -0.2 ADU/s, per 100 revolutions to ~ 0.00. In order to understand how much of the difference among the individual pixel gradients is real, and how much is due to fitting uncertainties, we repeated the regression analysis separately for two subsamples of equal sizes extracted from the whole sample (i.e. by selecting only odd number revolutions in one subsample, and even number revolutions in another). We found that the average uncertainty on the individual pixel gradients is only ~ 0.004 ADU/s per 100 revolutions, much smaller than the pixel-to-pixel variations, which then must be real. As a consequence, applying the same drift correction to all pixels cannot work.

The accuracy of this linear-fit characterization of the dark long-term drift can be estimated by computing the RMS variation of the dark current values of all pixels through the mission. The average per-pixel RMS of all *handover darks* is $\simeq 0.5$ ADU for both T_{int} , if we do not apply any correction for the long-term drift. After subtracting from the observed dark current values the fitted ones, the average per-pixel RMS of all *handover darks* is reduced to $\simeq 0.25$ ADU.

Other T_{int} 's are not well covered in the handover measurements. In particular, the handover measurements at T_{int} =0.28 and 10 s only started in revolution 764, and the time coverage is too limited to allow a proper characterization of the trend throughout the whole ISO mission. The situation concerning the T_{int} =20 s LW darks is even worse, no

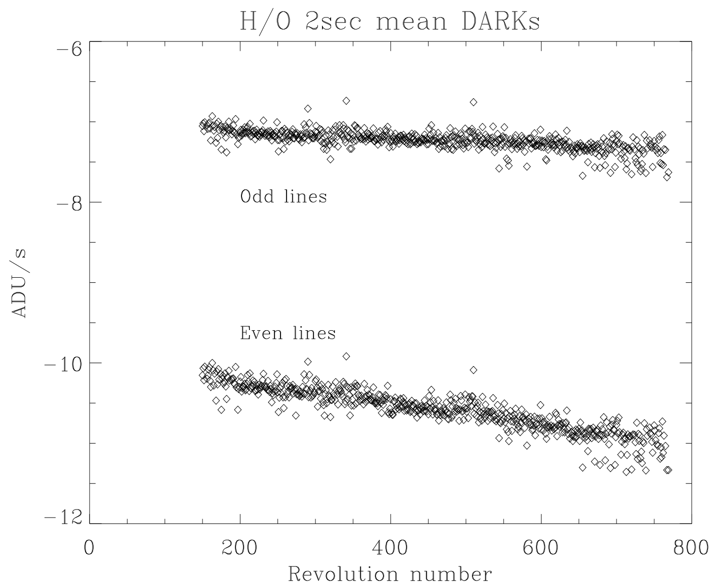

Figure 5: The mean values of the odd and even line pixel dark-currents as measured during the handover, vs. the revolution number, at T_{int} =2 s.

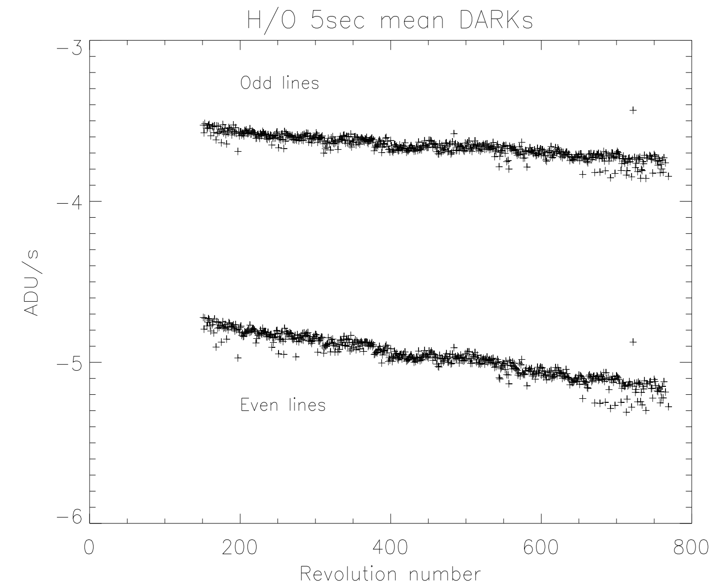

Figure 6: The mean values of the odd and even line pixel dark-currents as measured during the handover, vs. the revolution number, at T_{int} =5 s.

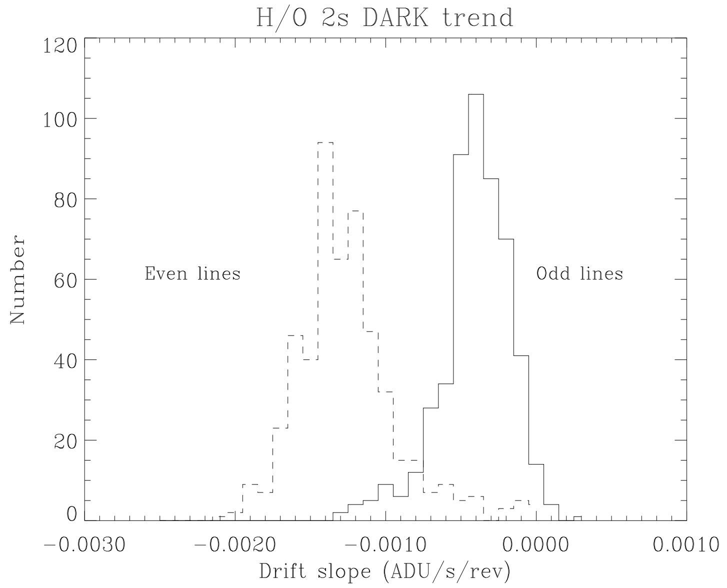

Figure 7: The distribution of individual pixel dark long-term drifts, at T_{int} =2 s, obtained by a straight line fitting of the observed value of the dark of each pixel vs. revolution number.

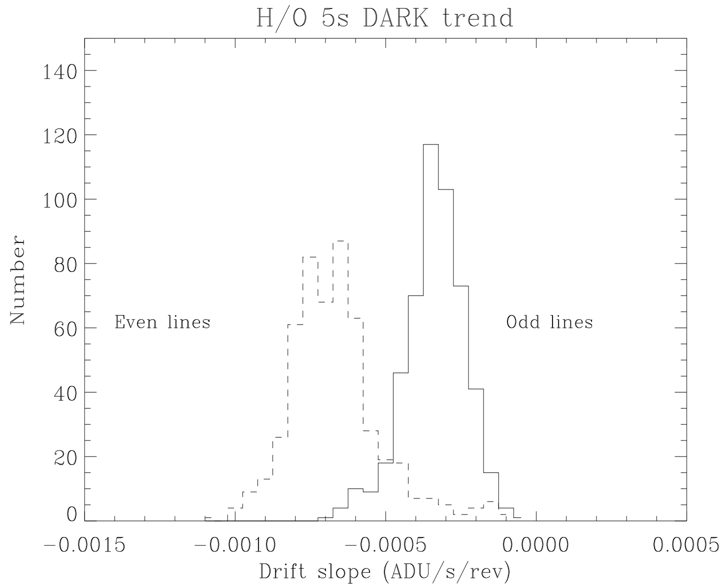

Figure 8: The distribution of individual pixel dark long-term drifts, at T_{int} =5 s, obtained by a straight line fitting of the observed value of the dark of each pixel vs. revolution number.

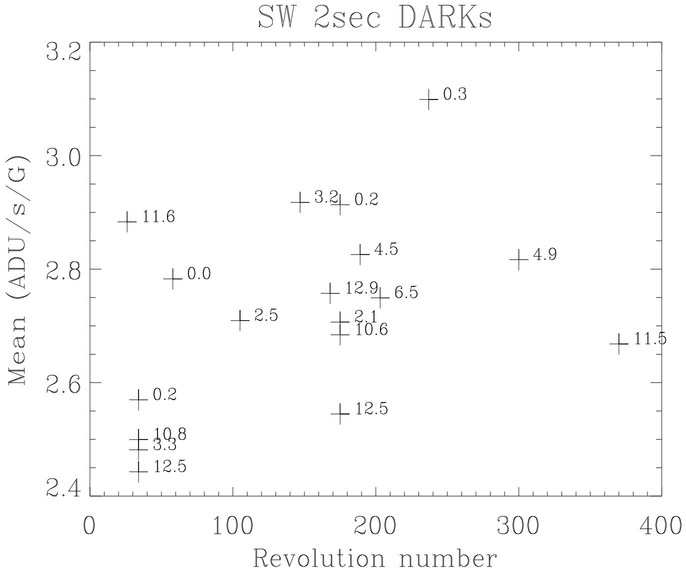

Figure 9: The mean dark current of the SW detector, measured at 2 s T_{int} in several calibration revolutions, vs. the revolution. Beside each point, the number indicates the time at which the observation was done in the revolution (in hours since the activation time).

measurement being done in handover for this integration time. However, it was possible to make use of the available *calibration darks* and *handover darks* to constrain the global trend, by *scaling* the linear-fits made on the 2 and 5 s measurements of *handover darks*.

We first checked that there was a global consistency among the long-term trends of the *handover darks* measured at T_{int} =2 and 5 s. Indeed it was found that by applying a suitable scaling factor one could deduce the trend at one T_{int} from the other. Then we checked that the 2 s long-term trend was consistent with the available data for *calibration darks* at T_{int} =0.28 s, and, correspondingly, that the 5 s long-term trend was consistent with the available data for *handover darks* and *calibration darks* at T_{int} =10 and 20 s. A global consistency was found. The scaling was then computed per pixel by averaging a set of measurements done at approximately the same time for the different T_{int} 's. Specifically, the dark currents at 0.28 s and 10 s were computed by averaging the handover measurements of revolutions 764 to 828. In order to obtain the scaling factors, they were divided by the dark currents at 2 s and, respectively, 5 s, computed by averaging the handover measurements of revolutions 765 to 829. The lack of handover measurements for the T_{int} =20 s dark did not allow to use measurements done at different T_{int} 's at the same time, so we simply used a global average of all available measurements.

For what regards the SW detector, unfortunately, no SW dark measurement is done during handover operations, so we must rely upon the poorer data-base of SW dark measurements done during calibration revolutions. In Fig. 9 we show the average SW dark current over the array vs. the revolution number; there is no firm evidence for a trend, and indeed a Spearman rank-correlation test fails to detect any significant correlation (at ≥ 90 % confidence level). In the figure we have also indicated, next to each point, the observation times, in hours since the time of activation of the instrument in each revolution (*time since activation, tsa* in the following). This could be interesting since, as we will see in § 5, both the SW and the LW darks show a drift with *tsa* , within a single revolution. Note, however, that this is of only limited concern for the *handover darks*, since they always occur at almost

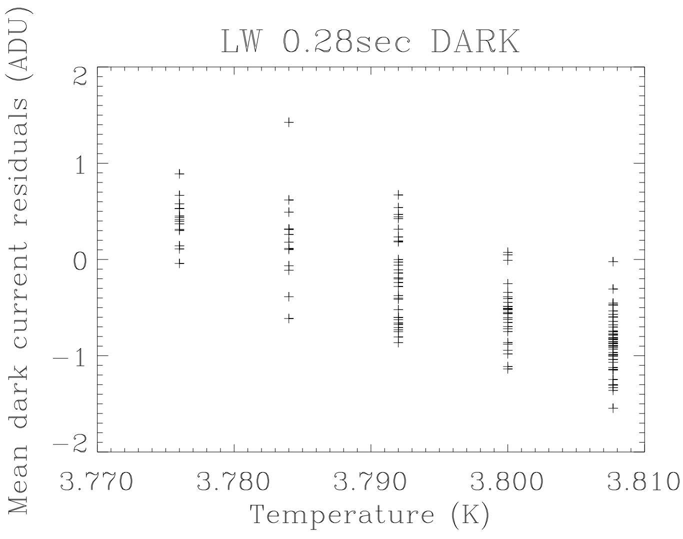

Figure 10: The correlation between the drift-corrected mean value of the LW dark current at T_{int} =0.28 s, as observed in several calibration revolutions, and the CAM detector temperature, in K.

the same *tsa* (the *tsa* 's of *handover darks* have an RMS of half an hour, and a peak-to-peak variation of less than 3 hours).

4 The temperature dependence

Once the dark measurements are corrected for the revolution drift, it is possible to show the existence of a relation between the mean dark current and the temperature of the CAM detector. This trend is shown in Fig. 10 for the T_{int} =0.28 s *calibration darks*, after correction for the long-term drift. At the current status of understanding, we can assume that the trend is the same for all pixels and at all T_{int} 's and can be described by a linear relation,

$$DARK_C = DARK_O - 66.119 + 17.467 \times T$$

, where T is the temperature in K, and $DARK_C$ and $DARK_O$ are the corrected and, respectively, observed value of the dark current, in ADUs.

Whether or not this relation also applies to the SW dark current is currently unknown.

5 Short-term drifts

The short-term drift of the dark current, repeating at each revolution, from the activation of the instrument to its deactivation, was first discovered in the *calibration darks*. At variance with the *handover darks*, the *calibration darks* span the full range of *tsa* . In some cases, several measurements were done during the same revolution at different *tsa* 's. It is then possible to look for the existence of a drift of the dark current with *tsa* [3].

[3]The choice of the activation-time for setting the reference time within each revolution *for what the dark short-term drift is concerned* is not unique. The perigee passage of ISO could as well have been chosen. In most revolutions, the time of activation is strictly related to the time of perigee passage, but in some it departs from the usual relation. In these, the short-term drift correction we have derived – described in this section – should be poorer than average, if the origin of time is not related to the activation, but, rather, to the perigee passage. This has yet to be tested.

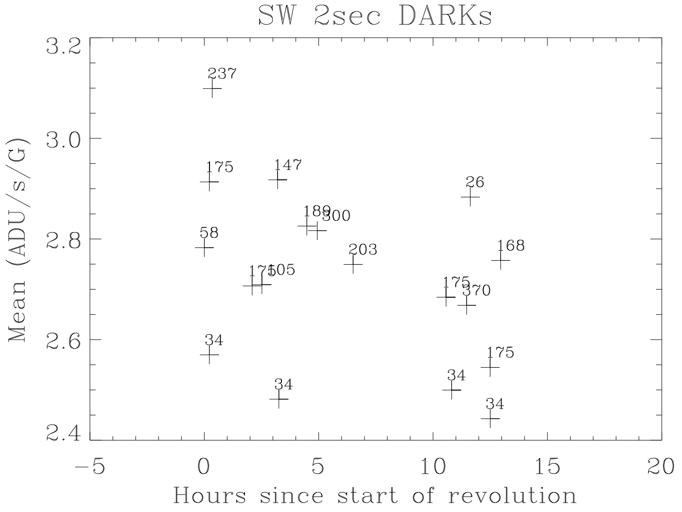

Figure 11: The mean dark current of the SW detector, measured at T_{int} =2 s in several calibration revolutions, vs. the *tsa* . Beside each point, the number indicates the revolution during which the observation was done.

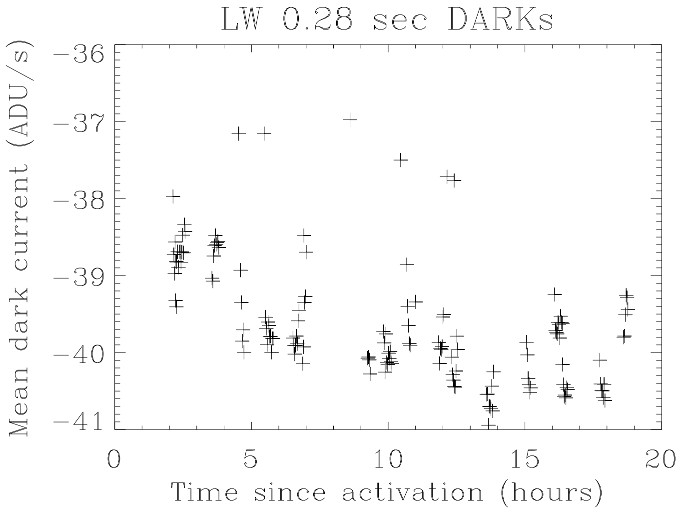

Figure 12: The mean dark current of the LW detector, measured at T_{int} =0.28 s in several calibration revolutions, vs. the *tsa* .

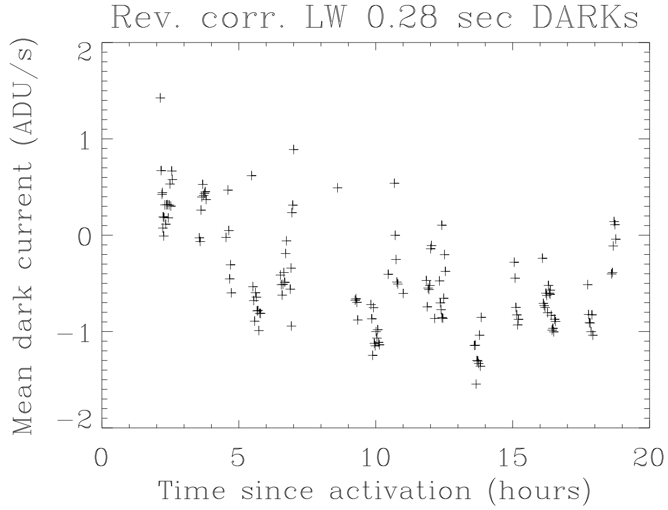

Figure 13: The mean dark current of the LW detector, after correction for the long-term trend, measured at T_{int} =0.28 s in several calibration revolutions, vs. the *tsa* .

In Fig. 11 we plot the mean dark current value of the SW detector, at T_{int} =2 s, as measured in several revolutions, vs. the *tsa* . Although not very significant (93 % confidence level, according to a Spearman test), there is a correlation between the two variables. The trend is even more evident for the LW detector, as can be seen in Fig. 12 for, e.g., the numerous T_{int} =0.28 s *calibration darks*.

Since the *calibration darks* are taken in different revolutions throughout the mission, the real trend may be masked by the long-term drift with revolution. For the SW darks we have labelled each point in Fig. 11 with the number of the revolution when the measurement was done; part of the scatter could indeed be due to a superposed long-term drift (e.g. note that the decreasing trend of the dark current in revolution 34 seems to be paralleled by the trend of the dark current in revolution 175). However, as discussed in § 3 it is impossible to correct for this long-term trend, because of the lack of data.

The long-term trend correction is instead feasible for the LW *calibration darks*. After subtracting the linear fit to the long-term trend of the *handover darks* (see § 3), the short-term trend with *tsa* is more evident (see Fig. 13; note that we also subtracted the temperature dependence, which, however, contributes less to the global scatter). Also in this case, the even and the odd lines show different behaviours, so that a proper characterization of the trend is only possible on a per pixel basis. As an example, we plot in Fig. 14 and Fig. 15 the trend of the mean dark current with *tsa* for the odd and, respectively, the even line pixels, and in Fig. 16 the trend of the difference of the two.

The *parallel-mode darks* also show the short-term drift very clearly. This is illustrated in Fig. 17, where the trend of the difference in the mean values of the dark current for odd and even pixels is shown, vs. *tsa* . The measurements were taken at T_{int} =5 s in three different revolutions. Note that superposed on the *tsa* -drift there is the long-term drift, so that each revolution short-term trend is a little bit shifted from the other.

The short-term drift appears to be as important as the long-term drift for the purpose of a correct calibration of the LW dark current behaviour. We made use of the *parallel-mode darks* for characterizing this trend for all T_{int} except for T_{int} =0.28 s, for which we used the *calibration darks* (*parallel-mode darks* are not available for this T_{int} , see § 1). Before making a fit of the dark current trends with *tsa* for each pixel, we had to subtract

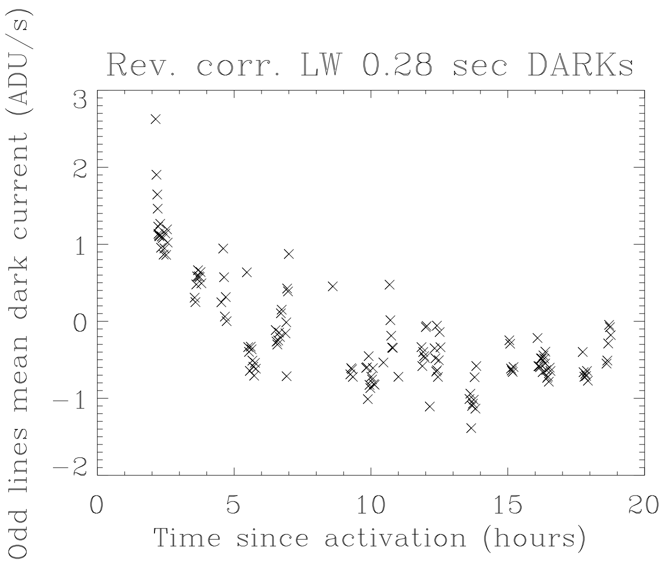

Figure 14: The mean dark current of the odd line pixels of the LW detector, after correction for the long-term trend, measured at T_{int} =0.28 s in several calibration revolutions, vs. the *tsa* .

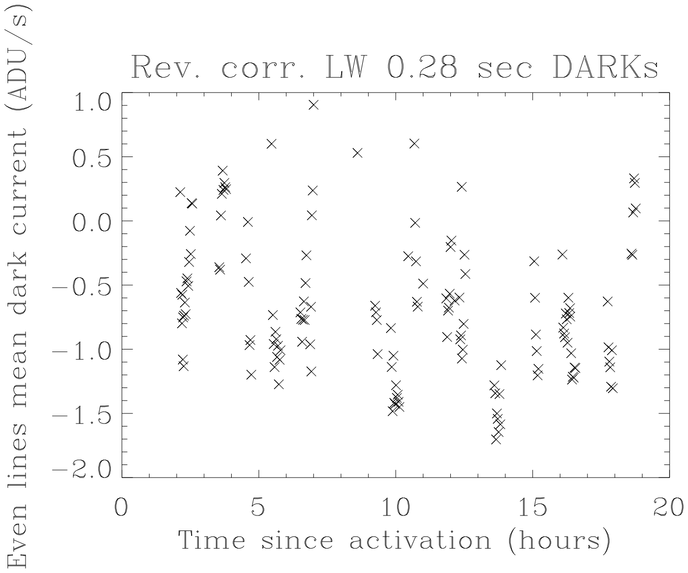

Figure 15: The mean dark current of the even line pixels of the LW detector, after correction for the long-term trend, and the temperature dependence, measured at T_{int} =0.28 s in several calibration revolutions, vs. the *tsa* .

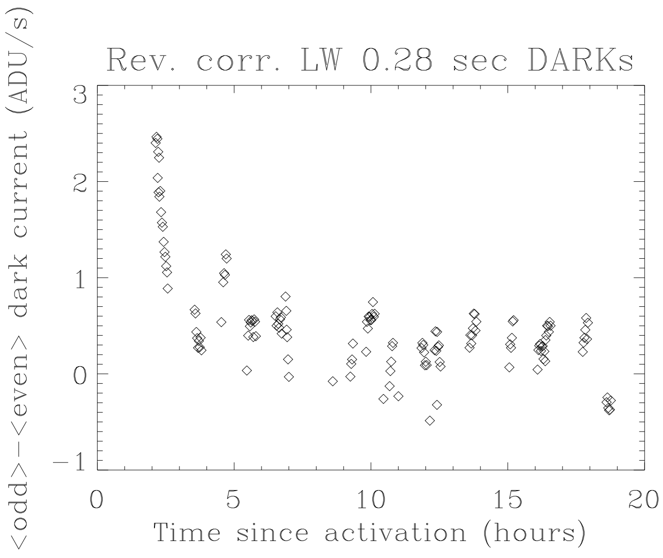

Figure 16: The difference of the mean dark currents of the odd and even line pixels of the LW detector, after correction for the long-term trend, measured at T_{int} =0.28 s in several calibration revolutions, vs. the *tsa* .

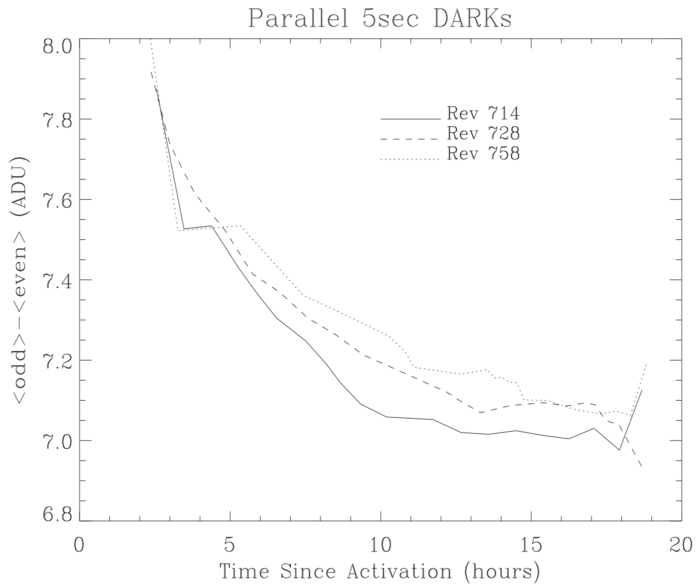

Figure 17: The (median-filtered) difference of the mean dark currents of the odd and even line pixels of the LW detector, measured in parallel mode at T_{int} =5 s in three revolutions, vs. the *tsa* . No correction for the long-term trend has been applied to the data, so that a shift is visible from revolution to revolution.

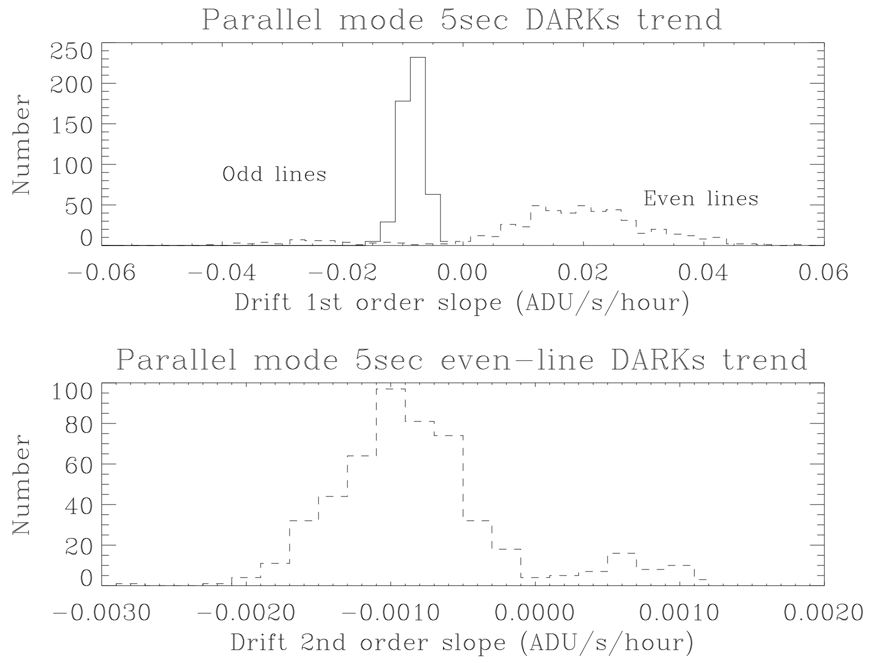

Figure 18: The distribution of the short-term drifts of the dark currents of individual pixel; note that the fits of the even-line pixel trends are quadratic, while those of the odd-line pixels are linear.

the long-term trend with the revolution number, described in § 3.

At variance with the long-term trend, it is clear that we cannot make a linear fit to the dark current short-term drift for all pixels. Some pixels required a quadratic fit, while for others a cubic fit was needed. More specifically, a cubic fit was found to be needed for properly describing the trend of the T_{int} =2 s dark current of even line pixels. Quadratic fits were needed for characterizing the short-term drifts of the dark currents of odd line pixels at T_{int} =0.28, 2 and 10 s, as well as that of the even line pixels at T_{int} =5 and 20 s. Finally, linear fits were adopted for all other pixels.

Note that the intercept of the fitting lines (or the zero coefficient of the polynomial fitting) is in general not zero. This is because the correction applied for the long-term trend was based on *handover darks* which have a slightly higher level than other dark measurements because of the different deglitching routine used in the data-reduction (see § 2.1). So, the application of the short-term drift correction also corrects for the slight systematic effect introduced by the long-term drift correction.

We show the results of the fitting of the short-term drifts of the dark current of individual pixels for T_{int} =5 s in Fig. 18. This is typical of other T_{int} 's as well, since the odd line pixels always show a decreasing trend with *tsa* , while the even line pixels have an increasing trend.

6 The accuracy of the calibration

As discussed in the previous sections, our calibration of the dark current for the LW detector takes into account both a long-term and a short-term drift (with a timescale of days, and respectively, hours), while, unfortunately, this was not possible for the SW detector. Our best estimate for the SW dark then simply comes from an average of all the available measurements. The accuracy of the calibration can be estimated from the median of the residuals after this average dark current frame is subtracted from all other SW dark measurements. The median residual is 0.46 ADU.

The LW reference dark image varies according to the revolution, the *tsa* and the focal-plane temperature. The precision of our calibration can be evaluated by computing the residuals of our model dark-subtraction from individual *calibration darks*. From all dark-subtracted dark measurements at a given T_{int} , we compute the per-pixel RMS. The median RMS is typically $\simeq 0.25$ ADU, similar to the one found for the *handover darks* without any temperature and *tsa* -drift correction, but after the long-term trend correction (see § 3). This is not unexepected, since the handover darks are all done at roughly the same *tsa* , so there is no need for correcting them for the *tsa* drift, and the temperature dependence is generally of minor importance as compared to the revolution and *tsa* drifts.

We can compare this time-dependent dark current correction with that obtained by a simple average of several dark-current measurements, i.e. the "calibration dark" that was used previously. The application of an unique average dark current correction would increase the median per-pixel RMS of the residuals to $\simeq 0.5$ ADU, i.e. twice the value we obtained above. This is illustrated in the following examples.

In Fig. 19 we provide an example of a specific calibration observation of a star, at T_{int} =2 s, reduced with an average dark subtraction, and with the drift-corrected time-dependent dark subtraction. The dark line pattern is evident in the image reduced with the average dark, implying an imperfect dark subtraction.

Another example is given in Fig. 20, where we show a science observation of a comet at T_{int} =0.28 s. Again, the dark line pattern is evident when we apply the average dark subtraction and not anymore when the drift-corrected dark model is used. To have a better quantitative feeling of the accuracy of the dark correction, we plot in Fig. 21 the flux observed after the two kinds of dark subtraction, along a single column, so to emphasize the line pattern. The residual is ~ 2 ADU/s (i.e. 0.6 ADU, since T_{int} =0.28 s) when the average dark subtraction is applied, while it is less than 1 ADU/s (~ 0.2 ADU) when the drift-corrected dark model subtraction is applied, consistently with the estimates given above.

As a final example, we show in Fig. 22 and Fig. 23 the final reduced images of an observation of a galaxy at 100 Mpc distance, done at 1.5″with the LW2 filter, T_{int} =2 s, in revolution 617. As before, we have used two kind of dark corrections: an average of several *calibration darks* in Fig. 22 and our drift-corrected dark model in Fig. 23. The dark subtraction is not perfect even when using the drift-corrected dark model, but it is anyway much better than the one obtained with a simple average dark.

7 Conclusions

We have shown that there are several effects that contribute to modify the dark current of the CAM detector during the ISO mission. In particular, we have identified:

- a *long-term drift,* i.e. a linear decrease of the dark current from a revolution to another, with a typical time-scale of days;
- a *short-term drift,* i.e. a modification of the dark current within a single revolution, from the beginning of the revolution to the end (we choose the activation of the instrument as the zero-point of the timescale within each single revolution); the modification of the dark current is in general non-linear, and does not show a unique monotonic behaviour for all pixels;
- a correlation of the dark current with the temperature of the CAM focal-plane; for the time being, and consistently with the analysed data, this correlation has been assumed to be unique, the same for all pixels, and at all T_{int} 's.

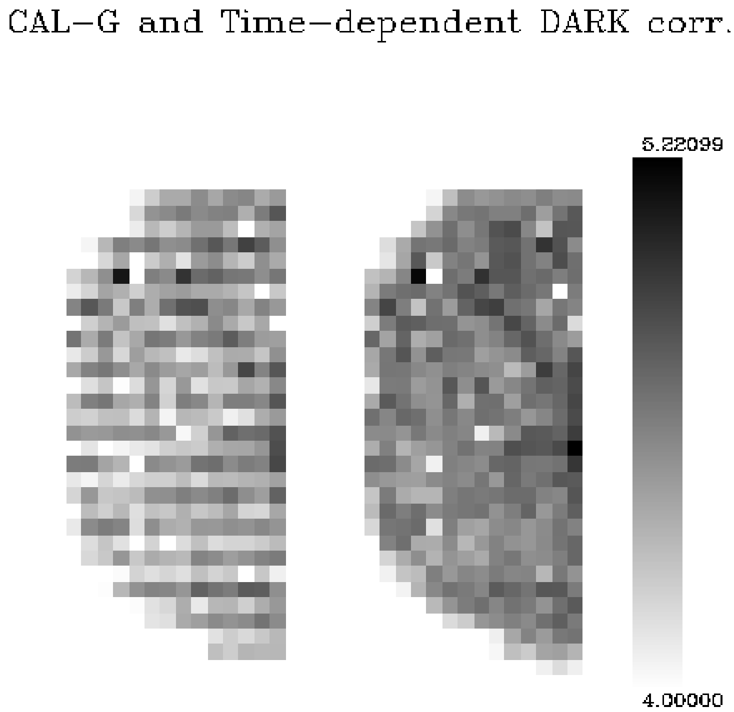

Figure 19: The calibration observation of the star HIC85317 done in rev.419, at 6.0″PFOV, and T_{int} =2 s, with the LW6 filter. reduced using an average dark subtraction (left) and with the time-dependent drift-corrected dark subtraction (right). Only half of the array is shown in both cases (the star itself is not visible, since it is located on the other half of the array). Flat-fielding was not applied, which explains the vignetting effect at the edges.

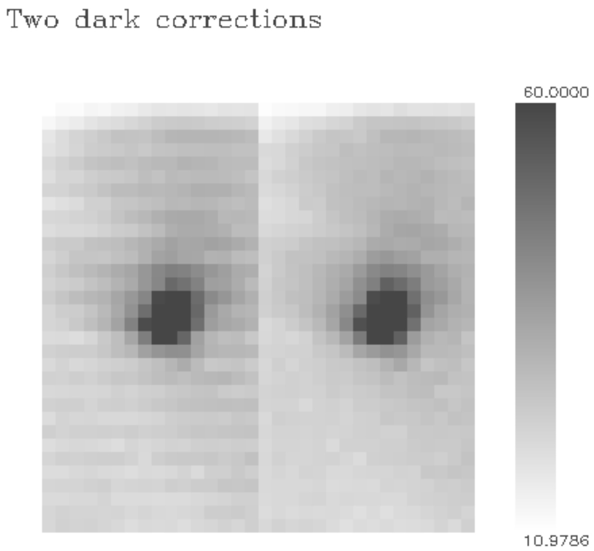

Figure 20: An observation of a comet done in rev.341, with T_{int} =0.28 s, with the LW9 filter, reduced using an average dark subtraction (left) and with the time-dependent drift-corrected dark subtraction (right). Only the central half of the array is shown in both cases. The images are shown before flat-fielding.

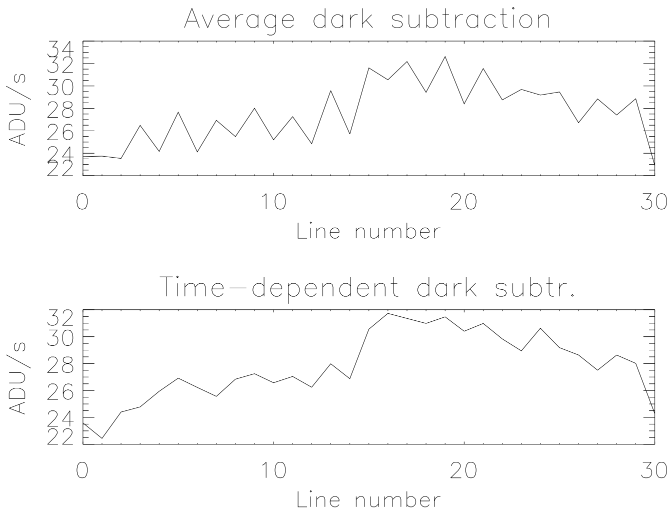

Figure 21: The flux along a single column of the comet observation shown in Fig. 20. Upper panel: after subtracting an average calibration dark. Lower panel: after subtracting the drift-corrected dark model.

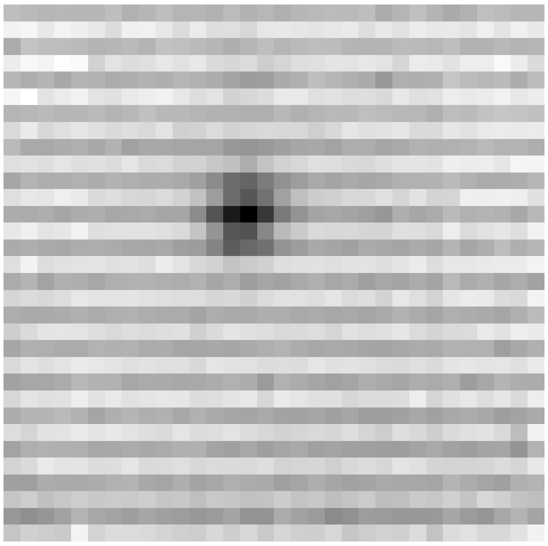

Figure 22: The final reduced image of an LW2 1.5″, T_{int} =2 s observation of a 100 Mpc distant lenticular galaxy. The dark used to produce this image is an average of several *calibration darks.*

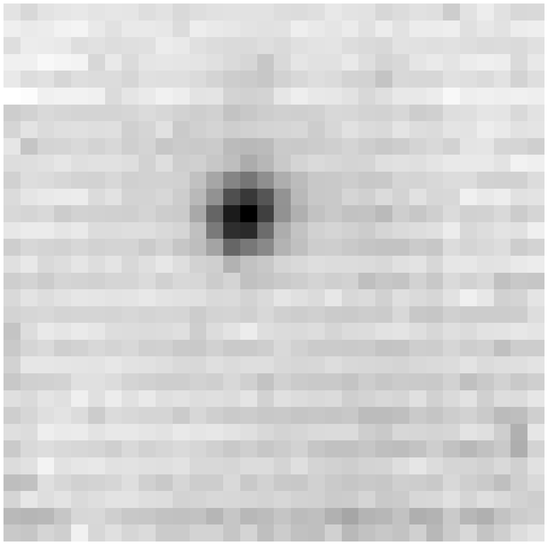

Figure 23: The final reduced image of the same observation of Fig. 22, where the drift-corrected dark model has been used instead of an average calibration dark.

All these effects are clearly established for the LW detector for which a sufficient amount of data is available. Some of these effects may also apply to the SW detector, but in this case the data are much sparser, and do not allow us to draw any conclusion.

For the LW detector, the impact of each of these effects on the dark-current can be summarized as follows:

- *long-term trend:* the drift is ~ -2 ADU from the beginning to the end of the ISO mission;
- *short-term trend:* the drift within each revolution is $\sim \pm 0.5$ ADU from activation to de-activation;
- *temperature-dependence:* ~ 0.5 ADU for the full range of temperature variation (few hundreths of a kelvin).

Correcting for all these effects is clearly important. We have modelled them using linear/quadratic/cubic fittings of the available dark current data, taken under many different conditions (during the handover, during prime-mode calibration revolutions, and with CAM operating in parallel-mode). The result is a dark-model, dependent on three variables: (i) the number of the revolution, (ii) the time of observation within that revolution (counted since the instrument activation), and (iii) the temperature of the CAM focal-plane. The dependence is different for different pixels, and slightly different for different T_{int} 's, although at our current level of understanding we cannot say if the T_{int} -dependence is really significant. Note that our current understanding of the temperature-dependence is that it is unique for all T_{int} 's and all pixels, at variance with the revolution and *tsa* dependences.

Once corrections are applied, the median LW dark current residual amounts to $\simeq 0.25$ ADU, which is even better than the pre-launch estimate of 0.3 ADU (Perault & Metcalfe 1995, see also Biviano 1998).

The lack of data has made these corrections impossible for the SW detector. This cannot be considered as a major fault in the CAM calibration strategy, because of the limited calibration time available, which had to be spent on the most used observing modes (the LW detector observations sum up to 97 % of the total CAM observations). However, even without any corrections for eventual drifts and/or temperature dependences, the dark current residual we get after using an average of all SW *calibration darks*, is consistent with the pre-launch estimate of 0.5 ADU (Perault & Metcalfe 1995, see also Biviano 1998).

The dark-model described in the previous section will become the standard dark-correction for CAM data-reduction in the latest versions of CIA and OLP (Ott et al. 1996, Siebenmorgen et al. 1998). As we have shown in § 6 this represents a significant improvement in the data-reduction, as compared to previous versions of CIA and OLP that were using an average of many *calibration darks* as the reference calibration dark.

References

Claret A. 1998,
Delaney M. 1997, "ISOCAM Interactive Analysis User's Manual", v.2.0
Gallais P. 1998, "Report on the trend analysis of the CAM daily calibration measurements"
Ott S. et al. 1996, "Design and implementation of CIA, the ISOCAM interactive analysis system", ASP Conference Series vol.125
Perault M., Metcalfe L. 1995, "Technical Note About the Error Budget Estimate in CAM Observations"
Siebenmorgen R., Starck J.-L., Cesarsky D.A., Guest S., Sauvage M. 1998, "ISOCAM data user's manual"

List of abbreviations and symbols

- ADU, ADU/G, ADU/g - Analog to Digital Unit, the unit of all CAM observations, scaled by the gain factor;
- g, G - Gain;
- PFOV - Pixel Field-Of-View;
- s, sec - second, unit of time;
- T_{int} - the integration time of a single frame exposure;
- *tsa* - the time of an observation in a given revolution, counted in hours since the activation of the instrument at the beginning of that revolution.